Adaptive deghosting for a rough and dynamic sea surface

Vrolijk, Jan-Willem; Blacquière, Gerrit

DOI
10.1190/segam2018-2998273.1

Publication date
2018

Document Version
Final published version

Published in
SEG Technical Program Expanded Abstracts 2018

Adaptive deghosting for a rough and dynamic sea surface

Jan-Willem Vrolijk and Gerrit Blacquière, Delft University of Technology*

SUMMARY

The sea surface is a strong reflector that results in a ghost wavefield at the source and the detector side. Consequently, a interference pattern occurs in the wavenumber-frequency domain. For a flat sea surface deep notch areas in the spectrum appear where there is destructive interference. The SNR (signal-to-noise ratio) is low in these areas. A rough and dynamic sea surface affects the propagation of the ghost wavefields and will distort the notch areas. If a rough and dynamic sea surface is present it should be taken into account in the process of deghosting. When the rough and dynamic sea surface is neglected the estimated ghost-free data will contain more noise. Often there are no additional measurements available that provide the exact shape of the rough and dynamic sea surface to model its corresponding ghost effect. Therefore, we introduce an adaptive deghosting method that takes into account a rough and dynamic sea surface without any prior information of this sea surface.

INTRODUCTION

Numerous deghosting algorithms make an effort to include the roughness of the sea surface. Some methods approximate the effect of the rough sea surface with an frequency and angle dependent reflectivity (Orji et al., 2013; Perz and Masoomzadeh, 2014). Other deghosting methods explicitly take into account the shape of the rough sea surface (King and Poole, 2015; Grion and Telling, 2017). In practise, often the shape of the rough and dynamic sea surface is unknown and even if the shape of the sea surface is estimated with a dedicated method (Laws and Kragh, 2002; King and Poole, 2015) it still contains uncertainties. These uncertainties will cause noise in the data after deghosting, that often appears as ringing (e.g. Egorov et al., 2018). A deghosting method should be adaptive to handle these uncertainties. In Rickett et al. (2014) such an adaptive algorithm is introduced that provides the optimal ghost delay times simultaneously with the deghosted data. The earlier mentioned methods are often developed for the τp-domain. The physics behind the ghost wavefield for a rough sea surface that causes different angles for the direct and ghost wavefield is more complex than the parameterisation of a ghost delay time in this domain. In this abstract the non-adaptive closed-loop deghosting method, which is based on wavefield propagation in the space-frequency domain (Vrolijk and Blacquière, 2017), is extended to an adaptive deghosting method. The distance between the sources and/or detectors and the local sea surface is adaptive during the deghosting to handle the uncertainties and account for lateral changes related to a rough and dynamic sea surface. The deghosting scheme can be applied to several temporal subsets of the data to handle the dynamic effect of a rough sea surface (Grion and Telling, 2017).

FORWARD MODELLING DETECTOR GHOST

First we introduce the forward model at the detector side. The depth of the cable is z_d, this could be a spatial dependent variable, given by $z_d = z_d(x,y)$. According to the matrix notation (Berkhout, 1985) the detector matrix including the detector ghost in the frequency domain can be written as:

$$\mathbf{D}(z_d) = \mathbf{D}_0(z_d)\mathbf{G}(z_d, z_d), \tag{1}$$

with $\mathbf{D}_0$ the ghost-free detector matrix. Here the ghost matrix at the detector side for a rough and static sea surface with a spatially variable level $z_0 = z_0(x,y)$ is given by:

$$\mathbf{G}(z_d, z_d) = \mathbf{I}(z_d, z_d) - \mathbf{W}^+(z_d, z_0)\mathbf{W}^-(z_0, z_d), \tag{2}$$

where $\mathbf{W}^-(z_0, z_d)$ describes forward propagation from the dectector level up to the sea surface and $\mathbf{W}^+(z_d, z_0)$ describes forward propagation from the sea surface down to the detector level, the minus sign represents the strong sea surface reflectivity of -1. The shape of the rough sea surface is explicitly taken into account in the forward propagation matrices. The dynamic effect of the sea surface needs to be included in the forward modelling at the detector side since detectors measure continuously, which means that $z_0 = z_0(x,y,t)$. We can repeat the forward modelling for many static sea surfaces ($i = 1, 2, ..., M$) to achieve this. One monochromatic shot record $[\vec{P}(z_d; z_0)]_i$ includes the ghost effect of a static sea surface corresponding to time instance i, which can be formulated as:

$$[\vec{P}(z_d; z_0)]_i = \mathbf{D}_0(z_d)[\mathbf{G}(z_d, z_d)]_i\mathbf{X}(z_d, z_0)\vec{S}_0(z_0), \tag{3}$$

with $\mathbf{X}$ the earth transfer function and $\vec{S}_0$ a vector with a single source distribution. The final shot record is obtained after an inverse Fourier transform and selecting the correct time instance related to each static sea surface (see Figure 1):

$$[\vec{P}(z_d; z_0, \omega)]_i \overset{\mathscr{F}^{-1}}{\Longrightarrow} [\vec{p}(z_d; z_0, t)]_i \Longrightarrow \vec{p}(z_d; z_0, t = t_i) \tag{4}$$

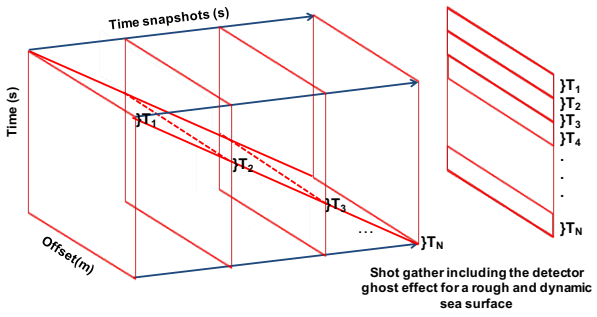

Figure 1: *The final shot record is composed from many time instances, each record contains the detector ghost wavefield for the static sea surface at that moment.*

10.1190/segam2018-2998273.1

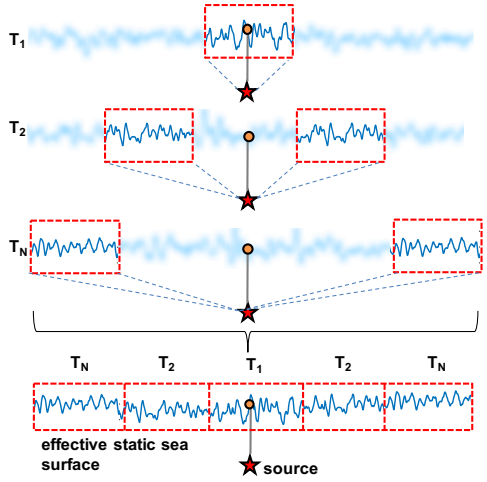

Figure 2: *The effective static rough sea surface is composed of parts of the sea surface that affect the source wavefield at a specific time.*

with ω is the frequency, $\mathscr{F}^{-1}$ is indicating the inverse Fourier transform, $\vec{p}$ is the shot record in the time domain and t_i the time instance related to the particular static sea surface at that time. The next shot is normally activated at a different time, at least in conventional marine seismic. Therefore, this modelling exercise is carried out per shot record.

FORWARD MODELLING SOURCE GHOST

We assume that the source is impulsive and properties for the up- and downward direction are the same and given by $\mathbf{S}_0$. Then the source matrix at tow depth $z_s = z_s(x,y)$ including the ghost effect $\mathbf{S}$ becomes:

$$\mathbf{S}(z_s) = \mathbf{G}(z_s, z_s)\mathbf{S}_0(z_s), \tag{5}$$

where $\mathbf{G}(z_s, z_s)$ is given by

$$\mathbf{G}(z_s, z_s) = \mathbf{I}(z_s, z_s) - \mathbf{W}^{+}(z_s, z_0)\mathbf{W}^{-}(z_0, z_s). \tag{6}$$

The rough and dynamic sea surface at the source side is approximated with an effective rough and static sea surface, because the upgoing wavefield is reflected from a certain area and at a specific time (see Figure 2). Obviously, each shot is emitted at a different time, meaning that the actual effective sea surface is different from shot to shot. A shot record including a source ghost that is related to an effective rough dynamic sea surface is given by:

$$\vec{P}(z_d; z_d) = \mathbf{D}_0(z_0)\mathbf{X}(z_0, z_s)[\mathbf{G}(z_s, z_s)]_j \vec{S}_0(z_s), \tag{7}$$

Finally, equation 7 can be easily extended to include the ghost response related to detectors at level $z_d(x,y)$ as well:

$$[\vec{P}(z_d; z_s)]_i = \mathbf{D}_0(z_d)[\mathbf{G}(z_d, z_d)]_i \mathbf{X}(z_d, z_s)[\mathbf{G}(z_s, z_s)]_j \vec{S}_0(z_s). \tag{8}$$

ADAPTIVE CLOSED-LOOP DEGHOSTING

We start with an adaptive closed-loop deghosting method that is able to handle a rough and static sea surface. Later, we include dynamic effects in this deghosting method. In the adaptive closed-loop deghosting method no prior information of the sea surface is required. Therefore, the initial source or detector depths with respect to the sea surface in the ghost model could be incorrect. The method will correct this by adapting parameter $\Delta z_d(x,y) = |z_d(x,y) - z_0(x,y)|$. The adaptive closed-loop detector deghosting method is based on minimizing the function:

$$\sum_{\omega} ||\vec{P}_j(z_d; z_s) - \mathbf{D}(z_d)\mathbf{X}(z_d; z_s)\vec{S}_j(z_s)||_2 \quad + \quad \lambda \sum_{t} ||\mathbf{x}(z_d; z_s)\vec{s}_j(z_s)||_1, \tag{9}$$

where $\mathbf{x}\vec{s}_j$ is the data without detector-ghost in the time domain, λ is a user-defined constant to set the level of sparsity, subscript 1 is indicating an L1-norm and subscript 2 is indicating an L2-norm. A gradient based method can be used to solve this underdetermined system for the deghosted data

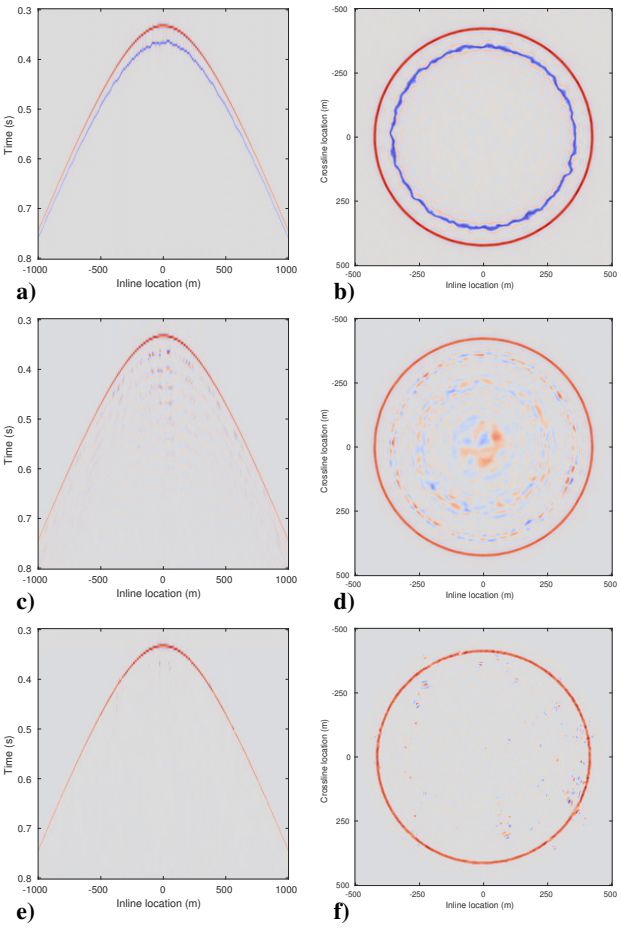

Figure 3: *Inline cross-section a) and time slice b) for a event and its corresponding ghost wavefield with detectors at* 30 *m for a rough sea surface. Inline cross-section c) and time slice d) after non-adaptive closed-loop deghosting. Inline cross-section e) and time slice f) after adaptive closed-loop deghosting*

10.1190/segam2018-2998273.1

$\mathbf{X}(z_d;z_s)\vec{S}_j(z_s)$ and Δz_d. In every iteration the gradient with respect to both variables is calculated. The gradient for parameter $\Delta z_d(x,y)$ is hidden in $\mathbf{D}(z_d)$ and in each iteration it is calculated with a first order approximation. Any prior information of the source and detector depths with respect to the shape of the sea surface obtained by other methods can be used as an initial estimate.

In order to handle the dynamic aspect of the sea surface, as described by Grion and Telling (2017), equation 9 is solved for several temporal subsets in a consecutive manner. Later (see Figure 4), we will validate this approach on a data set with a detector ghost wavefield that is modelled according to the forward model described earlier.

We can apply the deghosting method to a detector gather for source deghosting. As mentioned, for a single impulsive source, the dynamic property can be approximated by an effective rough and static sea surface. At the source side the source depth is more likely to vary with the sea surface, especially for an air-gun array that is floating, which means that the source depth is influenced by the rough sea surface. The deghosting method can handle a varying source and detector depth since the adaptive parameter is based on the difference with respect to the sea surface, given by variables Δz_d or Δz_s. In addition, when observed in a detector gather, the source ghost wavefield will contain jitter as the effective static sea surfaces could differ from trace to trace. This might restrict source deghosting for a rough sea surface, since wavefield propagation is not physically related to the source ghost wavefield that appears in a detector gather. Later (see Figure 5), we will test the source deghosting for the case of a effective mild and rough sea surface.

A single reflection event and its corresponding ghost wavefield are modelled for a 3D rough and static sea surface (Pierson and Moskowitz, 1964). The detectors are located on a plane at a depth of 30 *m*. Figures 3a and b show an inline cross-section and time-snapshot, respectively. At the near-offsets the irregular shape of the ghost wave is clearly visible in both cross-sections, for further offsets the effect will be less apparent due to wavefront healing. As a reference we show in Figures 3c and d the result after non-adaptive deghosting (Vrolijk and Blacquière, 2017). Figures 3c and d indicates that ignoring the rough character of the sea surface will introduce noise. In Figures 3e and f we see that a more accurate deghosting result is obtained with the adaptive deghosting method.

DEGHOSTING FOR ROUGH SEA SURFACE

Case I: Detector deghosting for a rough and dynamic sea surface

A finite difference scheme is used to generate the Earth transfer function (see equation 3). A rough and dynamic sea surface for an extreme sea state 9 is modelled according to Pierson and Moskowitz (1964). The ghost wavefield at the detector side (see equation 3) is modelled, corresponding to detectors around 30 *m* with a standard Kirchoff method (Laws and Kragh, 2002). The earlier mentioned forward model (see equations 3 and 4) is used to generate the shot record including the primaries, internal multiples and the dynamic detector ghost effect. In Figure 4a we show a magnified subdomain of the full shot record. As a reference the result after adaptive deghosting is shown in Figure 4c. The ghost model that comes out of this adaptive deghosting corresponds to a rough and static sea surface, i.e., the dynamic character of the sea surface has not been taken into account. Therefore, the artefacts in Figures 4c and e are mostly related to the fact that the sea surface is dynamic. The residual and corresponding SNR in Figure 4e are given with respect to the modelled data that are shown in Figure 4b. In Figures 4d and 4f we see that a more accurate deghosting result is obtained after applying the adaptive deghosting method including the dynamic effects with several temporal subsets. The SNR of the result of this window-based adaptive deghosting method is improved with more than 10 *dB* with respect to the SNR of the result after applying the adaptive method using a static assumption.

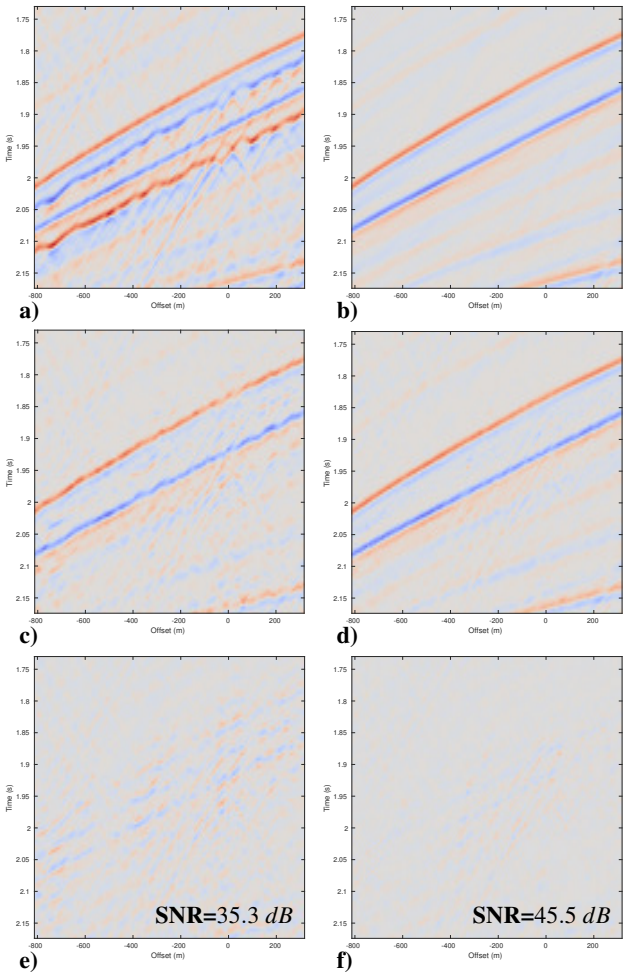

Figure 4: *Magnified shot gathers. In a) the input shot with ghost effect, detectors are at $z_d = 30$ m, b) modelled ghost-free data c) output after adaptive detector deghosting, d) output after window-based adaptive detector deghosting, e) residual after adaptive detector deghosting and f) residual after window-based adaptive detector deghosting.*

10.1190/segam2018-2998273.1

Case II: Source deghosting for effective rough sea surfaces

The Earth transfer function is again modelled with a finite difference scheme and for each shot record the source ghost matrix including the ghost wavefield is calculated for a rough sea state 6 and an extreme sea state 9. The detector gathers are selected from the full datasets with a source ghost that corresponds to sea state 6 (Figure 5a) and sea state 9 (Figure 5b). Each source has a depth of 20 m and its ghost wavefield is related to the effective static sea surface corresponding to its activiation time. This results in time jitter that becomes more clear in the extreme case (Figure 5b). Figures 5c and d shows that the deghosting result after the adaptive deghosting method for both sea states is pretty accurate. In Figures 5e and f we se the corresponding residual and SNR with respect to the ghost-free data set. These results indicate that even in a detector gather where the used wavefield propagation operator is not physically related to the total source ghost wavefield resulting in trace-to-trace jitter, the adaptive deghosting algorithm is able to remove the ghost wavefield accurately.

PRACTICAL APPLICATION IN 3D

The proposed 3D wavefield deghosting method requires a dense sampling in both the inline and crossline direction. Sun and Verschuur (2017) propose a 3D detector deghosting method for pressure data at the detector side that implicitly handles sparse data. A similiar approach can be followed to extend the closed-loop adaptive deghosting method for conventional 3D marine data. Because of their relatively dense source sampling, VSP and OBC data allow practical application of 3D source deghosting taking into account that a detector gather is not a physical domain where wavefield propagation occurs. However, in the synthetic example we showed that even in the presense of a rough sea surface most energy related to the ghost wavefield is removed.

In addition, we propose that the low frequencies are treated with special care in deghosting. Low frequencies suffer from the notch at 0 Hz. From the current focus on broadband acquisition and broadband (pre)processing, it is well-known that the low frequencies are very important: they reduce the sidelobes of the wavelet, enhance the seismic resolution and are needed in full waveform inversion (FWM) (ten Kroode et al., 2013). Moreover they play a crucial role in impedance estimation. Fortunately, those low frequencies (if present) are usually perfectly sampled, i.e., their sampling satisfies the Nyquist criterion. Therefore, the coarse sampling in conventional acquisition, in particular at the source side, is mostly affecting the mid and high frequencies. This is our current research focus.

CONCLUSIONS

The closed-loop deghosting method is extended to an adaptive deghosting method. We show that it is possible to correct uncertainties in the shape of a rough sea surface and yet accurately deghost the data. Using several temporal subsets further improves the performance in the case of a dynamic sea surface

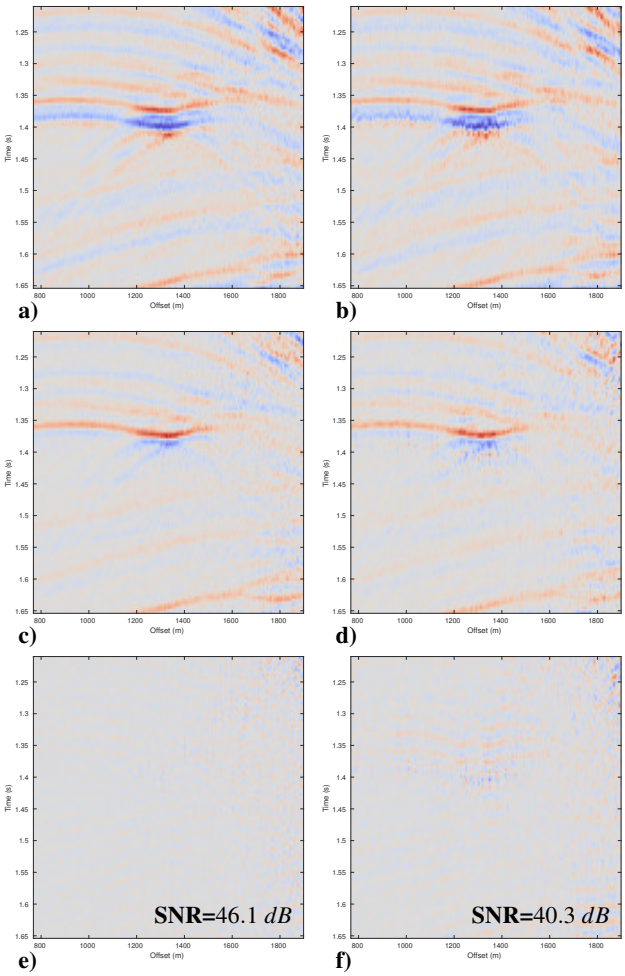

Figure 5: *Magnified detector gathers. In a) the detector gather with ghost effect for sea state 6, sources are at $z_d = 20$ m, b) the detector gather with ghost effect for sea state 9, sources are at $z_d = 20$ m c) output for a) after adaptive source deghosting, d) output for b) adaptive source deghosting, e) residual for c) after adaptive source deghosting and f) residual for d) after adaptive source deghosting.*

for detector deghosting. It is shown that the method can be used for adaptive source deghosting in the presence of an effective rough and static sea surface even though each trace of a detector gather is taken from a different shot record characterized by its own sea-surface shape. It is shown that the method can be applied in 3D, however, in practise the method will be restricted if the data is too sparsely sampled.

ACKNOWLEDGMENTS

We acknowledge the sponsors of the Delphi consortium for the stimulating discussions during the Delphi meetings and their continuing financial support support. We acknowledge Özkan Sertlek for generating the data in Figures 4a, 5a and b.

10.1190/segam2018-2998273.1

REFERENCES

Berkhout, A. J., 1985, Seismic migration. Part A: Theoretical aspects, 3rd ed.: Elsevier.

Egorov, A., S. Glubokovskikh, A. Bna, R. Pevzner, B. Gurevich, and M. Tokarev, 2018, How rough sea affects marine seismic data and deghosting procedures: Geophysical Prospecting, **66**, 3–12, https://doi.org/10.1111/1365-2478.12535.

Grion, S., and R. Telling, 2017, Estimation of a time-varying sea-surface profile for receiver-side deghosting: 87th Annual International Meeting, SEG, Expanded Abstracts, 4854–4858, https://doi.org/10.1190/segam2017-17742175.1.

King, S., and G. Poole, 2015, Hydrophone-only receiver deghosting using a variable sea surface datum: 85th Annual International Meeting, SEG, Expanded Abstracts, 4610–4614, https://doi.org/10.1190/segam2015-5891123.1.

Laws, R., and E. Kragh, 2002, Rough seas and time-lapse seismic: Geophysical Prospecting, **50**, 195–208, https://doi.org/10.1046/j.1365-2478.2002.00311.x.

Orji, O. C., W. Sollner, and L. J. Gelius, 2013, Sea surface reflection coefficient estimation: 83rd Annual International Meeting, SEG, Expanded Abstracts, 51–55, https://doi.org/10.1190/segam2013-0944.1.

Perz, M. J., and H. Masoomzadeh, 2014, Deterministic marine deghosting: Tutorial and recent advances: Presented at the FOCUS Geoconvention Abstracts, EAGE.

Pierson, W. J., and L. Moskowitz, 1964, A proposed spectral form for fully developed wind seas based on the similarity theory of S. A. Kitaigorodskii: Journal of Geophysical Research, **69**, 5181–5190.

Rickett, J., D.-J. V. Manen, P. Loganathan, and N. Seymour, 2014, Slanted-streamer data-adaptive deghosting with local plane waves: 76th Annual International Conference and Exhibition, EAGE, Extended Abstracts, 4221–4225, https://doi.org/10.3997/2214-4609.20141453.

Sun, Y., and D. Verschuur, 2017, 3D receiver deghosting for seismic streamer data using L1 inversion in an extended Radon space: 87th Annual International Meeting, SEG, Expanded Abstracts, 4940–4944, https://doi.org/10.1190/segam2017-17335240.1.

ten Kroode, F., S. Bergler, C. Corsten, J. W. de Maag, F. Strijbos, and H. Tijhof, 2013, Broadband seismic data—The importance of low frequencies: Geophysics, **78**, no. 2, WA3–WA14, https://doi.org/10.1190/geo2012-0294.1.

Vrolijk, J. W., and G. Blacquière, 2017, Deghosting and its effect on noise: 79th Annual International Conference and Exhibition, EAGE, Extended Abstracts, WE P5 12, https://doi.org/10.3997/2214-4609.201701400.